

## Research Paper

# Remotely-sensed evapotranspiration for informed urban forest management



Heng Wan<sup>a</sup>, Daniel McLaughlin<sup>b,\*</sup>, Yang Shao<sup>a</sup>, Brian van Eerden<sup>c</sup>, Shyam Ranganathan<sup>d</sup>,  
Xinwei Deng<sup>d</sup>

<sup>a</sup> Virginia Tech, Department of Geography, 238 Wallace Hall, Blacksburg, VA 24061, USA

<sup>b</sup> Virginia Tech, Department of Forest Resources and Environmental Conservation, 313 Cheatham Hall, Blacksburg, VA 24061, USA

<sup>c</sup> Virginia Pinelands Program, The Nature Conservancy, USA

<sup>d</sup> Virginia Tech, Department of Statistics, 211 Hutcheson Hall, Blacksburg, VA 24061, USA

## HIGHLIGHTS

- Remotely sensed evapotranspiration observations demonstrate clear differences among land cover types.
- Urban forest evapotranspiration exceeds other urban cover types and potentially provides important flood reduction services.
- Findings can help to guide green infrastructure design in our study area and other flood-prone urban settings.

## ARTICLE INFO

### Keywords:

Flood reduction  
Stormwater  
Green infrastructure  
Forest conservation

## ABSTRACT

With higher evapotranspiration (ET) rates compared to other urban land covers, urban forests can play an important role in stormwater flood reduction. Effective incorporation of urban forests into stormwater planning and green infrastructure design requires methods that can quantify ET across mixed-land use landscapes but with sufficient spatial resolution for parcel-specific rates. We used Landsat-derived ET from 2000 to 2018 to estimate 30-m annual ET rates across the City of Virginia Beach, USA, a large urban landscape with increasing flood concerns. Our objectives were to compare ET rates across land covers and then identify land attributes and models to explain spatial ET variation. Upland and wetland forests had higher ET compared to urban areas, where wetland forest had annual ET rates 3–4 times that of urban and contributed ca. 40% of total landscape ET despite covering only 20% of the area. These quantified ET rates highlight the disproportional role that urban forests may play in stormwater runoff reduction, and can inform scenarios of land use change to prioritize forest conservation efforts. Relationships between ET rates and aggregated, higher resolution land attribute data indicated key drivers, where ET increased with canopy cover and decreased with impervious cover and water table depth. A regression model combining these drivers explained approximately 70% of ET variation, providing means to downscale ET estimates to further guide stormwater planning at finer spatial scales. Our findings emphasize the importance of urban forests as green infrastructure elements and point to potential approaches to better incorporate them in stormwater planning decisions.

## 1. Introduction

Evapotranspiration (ET) is an important component in the hydrologic cycle and represents a major water loss in the landscape (Irmak & Haman, 2003; Rothfuss et al., 2010). Regional ET differences are largely driven by climate variables such as temperature and humidity (e.g., potential evapotranspiration; PET) (Teuling et al., 2009; Adnan, Ullah,

Khan, & Gao, 2017). However, local ET can vary widely based on land cover, vegetation types, and available water (Zhang, Dawes, & Walker, 2001) and thus particularly in mixed-land use landscapes. In urban settings, ET is generally much lower compared to less disturbed landscapes (Taha, 1997; Liu et al., 2010), which together with limited soil water infiltration results in increased stormwater flooding (De Roo, Schmuck, Perdigao, & Thielen, 2003; Berland et al., 2017; Kuehler,

\* Corresponding author.

E-mail address: [mclaughd@vt.edu](mailto:mclaughd@vt.edu) (D. McLaughlin).

Hathaway, & Tirpak, 2017). However, urban and suburban landscapes often contain a variety of land covers, which can substantially vary in ET rates, ranging from urban and residential covers to open greenspace, waterways and vegetated patches (Litvak, Manago, Hogue, & Pataki, 2017). Within these cover classes, drivers of ET can further exhibit spatial heterogeneity. For example, urban covers vary in impervious extents and structure heights, which can affect heat and turbulence fluxes and water availability (Grimmond & Oke, 1991; DiGiovanni-White, Montalto, & Gaffin, 2018 and references therein). Open space and vegetated patches typically support higher ET rates, which can be further increased due to the oasis effect (i.e., dry, hot air from impervious covers into vegetated areas; Drexler, Snyder, Spano, & Paw U, 2004), but can also exhibit ET variation due to differences in water availability and vegetation structures, ranging from turf grass to forest patches (Peters, Hiller & McFadden, 2011; Nouri et al., 2016). Quantifying such variable ET rates is thus needed to inform planning efforts and green infrastructure design that recognize the role of ET losses in flood reduction services.

Numerous studies document the use of green infrastructure (e.g., green roofs, vegetated swales, green spaces) in urban flood reduction (e.g., Lennon, Scott, & O'Neill, 2014; Liu, Chen, & Peng, 2014). Until recently, however, green infrastructure practices have mainly focused on infiltration-based technologies (e.g., rain gardens, permeable pavements) and individual “street” tree planting and conservation. Larger, urban forest patches can be a common feature embedded within otherwise mostly urban areas (Nowack, Noble, Sisinni, & Dwyer, 2001; see inset in Fig. 1), and thus deserve more attention as a green component due to their potentially higher water storage capacity (e.g., via canopy interception and soil infiltration) and subsequent water losses via ET (Berland et al., 2017). While it is not surprising that vegetated patches within urban and suburban settings can provide ET hotspots (Peters et al., 2011; Litvak et al., 2017), research is needed on urban forest ET relative to other surrounding cover types (Kuehler et al., 2017)

and at land-parcel scales (e.g., < 1 ha; Berland et al., 2017), a spatial scale necessary to inform stormwater planning decisions and green infrastructure design.

In situ methods for ET measurement (e.g., eddy covariance towers, sap flow sensors, and lysimeters) are costly and limited in spatial representation (Drexler et al., 2004; Glenn et al., 2011), and thus unfeasible for applications in heterogeneous systems such as urban landscapes (Nouri et al., 2020). In contrast, remotely sensed-based approaches can estimate ET at high spatial resolution while also covering large spatial extents (Courault, Seguin, & Olioso, 2005; Gowda et al., 2007). While remotely sensed methods have predominantly been applied in agriculture and more natural landscapes, they have been increasingly used in mixed-land use and urban settings (Nouri et al., 2016; Faridatul, Wu, Zhu, & Wang, 2020). For example, annual ET rates based on vegetation index methods and derived from MODIS satellite imagery can provide accurate estimates in mixed land uses but at a fairly coarse resolution (250 m), thus limiting finer scale information into spatial variability (Nouri et al., 2016). Using Landsat imagery data and an energy balance-based approach, the Mapping Evapotranspiration at high Resolution with Internalized Calibration (METRIC) model offers an alternative method to provide higher resolution (30 m) ET estimates (Allen et al., 2007; Trezza, Allen, & Tasumi, 2013; French, Hunsaker, & Thorp, 2015). The METRIC model and similar energy-based approaches have been widely used in agriculture settings, but some research has extended applications to mixed-land use and urban landscapes (Allen et al., 2007; Liu et al., 2010; Senay, Friedrichs, Singh, & Velpuri, 2016; Spiliopoulos, Holden, & Loukas, 2017; Faridatul et al., 2020). While there have been suggested refinements to these energy balance-based methods for focused applications in urban settings (Zhang et al., 2017; Faridatul et al., 2020), 30-m METRIC ET data are now readily available from the Earth Engine Evapotranspiration Flux (EEFLUX) tool on the Google Earth Engine Platform. As such, available METRIC data along with detailed land cover data may support broad inquiry into the relative ET

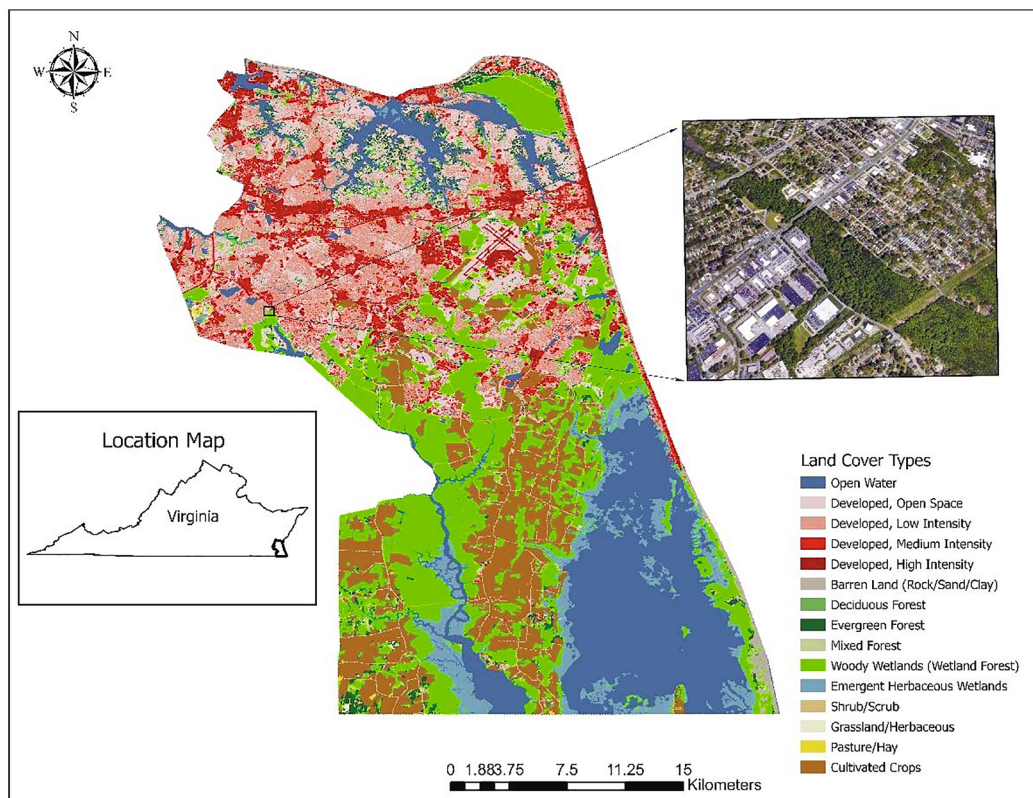


**Fig. 1.** Study area along with land use/land cover data from National Land Cover Database 2011. Insets show i) regional location and ii) characteristic upland and wetland forested patches within the otherwise urban landscape (from Google Earth Imagery).

differences between urban forests and other land covers and thus potential consequences of various land change scenarios.

In urban and suburban settings, remotely sensed ET values, including 30-m METRIC data, intrinsically represent mixed signals from sub-pixel cover components (Wu and Murray, 2003; Shao, Li, Guenther, & Campbell, 2015). Statistical modeling of ET using aggregated, higher resolution (e.g., 1-m resolution) land cover data can improve our understanding of ET drivers in urban settings and potentially enable downscaling of ET estimates. However, such modeling has been limited or conducted with larger analytical units (e.g., watershed scale and regional scale) (Kişi, 2006, 2011; Lu, Sun, McNulty, & Amatya, 2003; Sanford & Selnick, 2013), highlighting research needs to link ET and high-resolution land use data to inform green infrastructure planning at finer spatial scales.

Here, we use available METRIC 30-m ET data to compare annual ET rates among land cover types in Virginia Beach, USA. Using higher-resolution land use (0.5 m) and groundwater (3 m) data, we also explore potential drivers and associated predictive models of annual ET rates. We focus on Virginia Beach because the area has growing concerns related to stormwater flooding and increasing efforts to incorporate a

portfolio of solutions, including green infrastructure, for flood reduction. Understanding ET differences and associated drivers among land cover types will help such efforts in Virginia Beach and is broadly relevant to green infrastructure design and forest conservation in other urban landscapes.

## 2. Methods

### 2.1. Study area

The City of Virginia Beach encompasses ca. 640 km<sup>2</sup>, with a population of 450,189 as of 2018 and with an estimated 2.8% increase in population since 2010 (U.S. Census Bureau). According to the National Land Cover Database (NLCD) 2011, Virginia Beach land cover types include (Fig. 1): urban (“developed”) (39.3%), forested (“woody”) and herbaceous wetlands (28.3%), water bodies (12%), agricultural (14.1%), upland forests and shrubs (4.8%), and minimal amounts of other covers (e.g., grasslands & barren land). By comparing NLCD2001 and NLCD2011 datasets, the newly urbanized area in this decadal time period was approximately 13 km<sup>2</sup>, with a slow annual urbanization rate

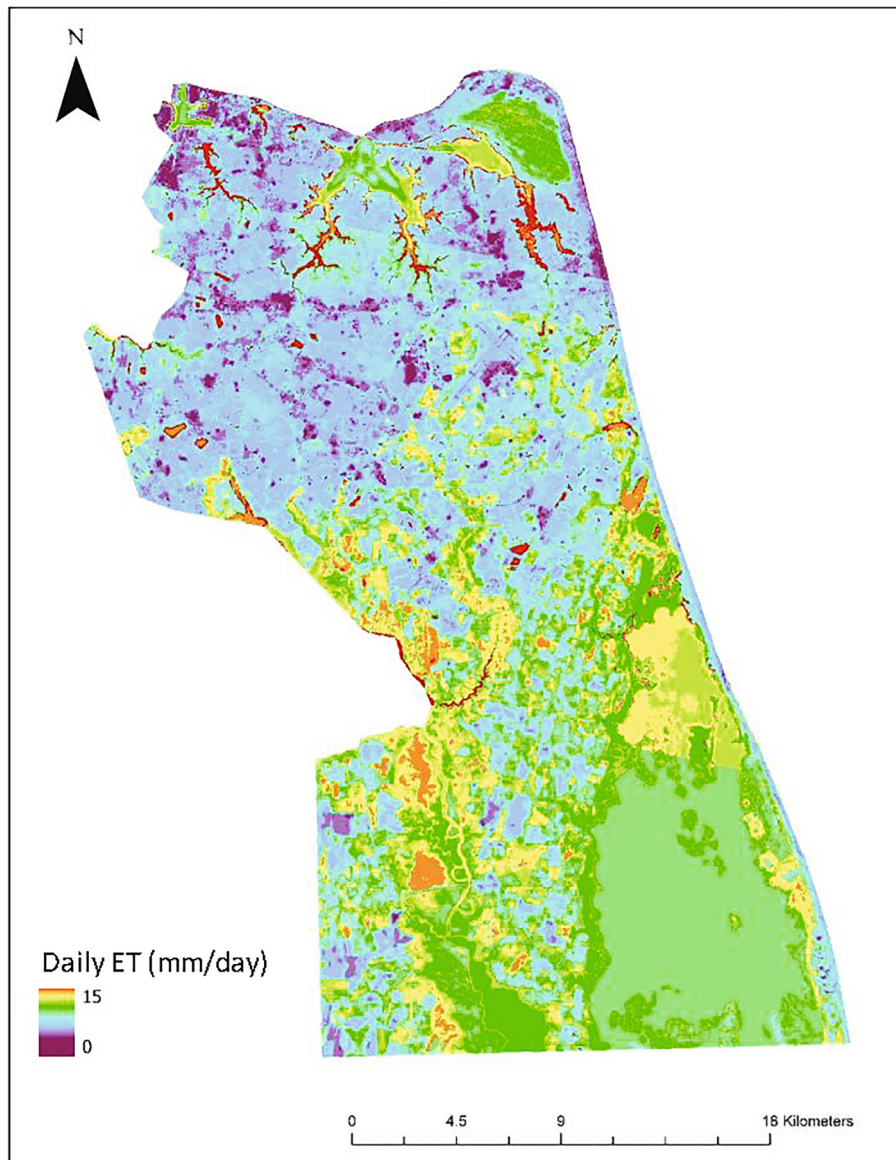


**Fig. 2.** Example of METRIC-derived daily ET from Landsat flyover on March 14th, 2013, obtained from EEFLUX.

(<1%). Soils in the study area are dominated by silt loam or loam (50% of the area), with smaller extents of sandy clay loam (35%) ([NRCS SSURGO Database](#)). The landscape is relatively flat, with a mean slope of 2.4%. The climate is considered humid subtropical, with annual precipitation of 1143 mm and annual potential evapotranspiration (PET) of 838 mm (for nearby Norfolk; Univ. of Virginia Climatology Office).

## 2.2. Data processing

### 2.2.1. Pre-processing METRIC-derived daily ET rates

To estimate ET across our study area required remotely sensed data that cover the required spatial scale as well as include enough observations over time to determine annual ET rates while accounting for seasonal variability. To do so, we obtained available ET data from the Earth Engine Evapotranspiration Flux (EEFLUX) tool, which estimates and calibrates ET data using the METRIC model and Landsat imagery archived on Google Earth Engine Platform ([Allen et al., 2015](#)). The model estimates daily ET (mm) at a 30-m resolution for each satellite fly-over date (16-day frequency); see example of daily ET observations in [Fig. 2](#), indicating lower ET values in northern, more urban locations ([Fig. 1](#)). The METRIC model is based on the previous Surface Energy Balance Algorithms for Land (SEBAL) model and is a mature, operational surface energy balance model capable of producing reliable ET estimation with high resolution for large spatial scales ([Allen et al., 2011](#); [Foolad et al., 2018](#)).

Daily ET data for 30-m pixels between 2000 and 2018 were downloaded from EEFLUX website (<https://eeflux-level1.appspot.com/>). Our study area encompasses two Landsat scenes, thus daily ET data for each scene were downloaded separately and then merged into one integrated dataset. These daily ET data were then manually checked to exclude scenes with a total cloud coverage over 30%, as reported in the EEFLUX output data. For the remaining scenes ( $n = 301$ ), we downloaded the corresponding original Landsat scenes (Landsat Level 1 collection products, including 5, 7, and 8 imagery) from Earth Explorer (<https://earthexplorer.usgs.gov/>). Then, these Landsat imagery data were processed by Fmask 4.0, a software capable of recognizing clouds and shadows, to generate cloud masks ([Qiu, Zhu, & He, 2019](#)). The daily ET data and their corresponding cloud mask were integrated to exclude cloud-contaminated pixels, providing a time series of cloud-free daily ET data for each 30-m pixel.

### 2.2.2. Determination of annual ET rates

Before deriving annual ET rates, cloud-free daily ET data were further processed to exclude outliers and decrease uncertainty in two steps. First, outliers were corrected by truncation using the long-term temporal distributions for each pixel, with the reasonable daily ET value range for each pixel defined based on the interquartile range rule. All the daily ET values beyond this reasonable range were regarded as outliers, which were reclassified as the corresponding upper/lower limit value. Second, to reduce uncertainty for pixels with limited or highly variable observations in a specific month, processed data were further corrected by borrowing strength from other pixels from the same land cover and month using Bayesian Posterior Processing (see S1).

With corrected daily ET rates, we determined average daily ET for each pixel and month using data between 2000 and 2018; these month-specific daily means were then converted to average annual rates (mm/year) for each pixel using number of days in each month. Annual means were compared among five major land cover types, as well as sub-categories within urban and forested categories. We note that removing cloudy days and pixels was a necessary step (due to increased uncertainty under such conditions; [Chen & Yang, 2012](#); [Hwang & Choi, 2013](#)) but results in a consistent bias to high (cloud-free) ET days. As such, derived annual estimates are likely overestimated; however, relative comparisons among land cover types should not be affected since this bias is equally applied across all pixels and land cover types.

## 2.3. Exploring ET changes due to land use change

The data range used here (2000–2018) was chosen to maximize data availability. For pixels experiencing land use (and associated ET) changes over this period, average annual ET rates from the full data range may not reflect current conditions. However, a comparison of NLCD 2001 and NLCD 2011 datasets demonstrated a slow annual urban growth rate (<1%) in our study domain, suggesting that generating the annual ET layer based on ET data from 2000 to 2018 is reasonable. Still, we did compare average annual ET separately for the 2000–2010 and 2010–2018 periods to explore potential changes in ET due to land use change over time. To do so, we identified two groups of pixels: ones that changed from a non-urban cover to an urban cover (i.e., newly urbanized) and those that did not experience land use change between the evaluated time periods. Differences in annual ET between the two time periods were then compared between the two groups using the non-parametric Mann-Whitney-Wilcoxon Test.

## 2.4. Drivers and models of annual ET

To explain ET differences among pixels, we obtained land attribute data for expected drivers, including impervious cover, canopy cover, and depth to water table. These data are available at higher resolution than the ET data, allowing us to understand aggregate controls on 30-m ET observations. For impervious cover and canopy cover, we used 0.5-m resolution land cover data acquired from the Tree Canopy Assessment for Virginia Beach ([O'Neil-Dunne, 2019](#)). In addition to higher resolution, these land cover data are also independent observations from Landsat imagery (used for NLCD datasets), from which our derived ET were based. Pixels (0.5 m) defined as urban were considered as impervious, and forested pixels were considered as canopy. These cover classes were then resampled to 30-m resolution, concordant with ET data, where percent canopy and impervious covers for each 30-m pixel were determined as the proportion of respective 0.5-m subpixel cover classes. For depth to water table, we combined LiDAR-derived bare earth digital elevation model (DEM) (3-m spatial resolution) from Virginia Information Technologies Agency (VITA; <https://www.vita.virginia.gov/integrated-services/vgin-geospatial-services/elevation-lidar/>) and USGS groundwater well observations (<https://waterdata.usgs.gov/va/nwis/gw>) to construct an interpolated 3-m raster set. To do so, we used 10 USGS wells, which had (sub-daily) data from 2012 to 2016, and calculated mean annual water table depth for each well. Using ground elevation of each well (from the LiDAR DEM), we then converted the mean annual water table depth at each well to water level elevation. Mean water level elevations were then spatially interpolated among well locations using inverse distance weighted interpolation, which is preferred when spatial autocorrelation exists and there are relatively few data points for interpolation ([Dormann et al., 2007](#); [Laguech, 2006](#)). The interpolation of water elevations produced a continuous groundwater layer for the entire study domain, which together with the DEM, was used to calculate a mean annual depth to water table for each 3-m pixel. These data were then resampled to 30-m by taking the average of 3-m values within each 30-m pixel, again concordant with the ET data. While the well data used spanned only a portion of our ET data record, relative spatial differences in water table conditions (and thus water availability) are useful when examining the degree to which they explain spatial differences in annual ET rates derived from longer time periods.

For each dataset, we conducted regression analysis using all pixels ( $n = 754$ ), with annual ET (for the full data record, 2000–2018) as our response variable. We report the significance and goodness-of-fit ( $R^2$ ) for these relationships using the full dataset but also illustrate the general trend in pairwise plots using a subset of 200 pixels, which were randomly sampled and equally ( $n = 50$ ) from each of four major land use categories: urban, upland forest, wetland forest, and agriculture. We also conducted multiple regression using the full dataset to develop a

predictive model of ET using all three expected drivers. To address potential nonlinearity, we explored several functional forms for both separate and multiple regression models, including linear regressions with different transformation methods (logarithmic, inverse, exponential, and box-cox transformations) and quadratic polynomial regression.

### 3. Results

#### 3.1. Annual ET comparison among land covers

**Fig. 3** illustrates the distribution of annual ET values from all pixels and categorized by major land cover types. Differences among land cover types are distinct, with wetland forest having the highest annual ET while urban cover has the lowest.

Urban land uses have the lowest average annual ET rates and thus contribute only 23% of the total landscape ET, despite disproportionately higher amounts of area coverage (45%) (**Table 1**). Mean upland forest annual ET is almost twice that of urban, but with its very low coverage (5.5%) contributes the least to the total cumulative ET (4.7%). Among all the land cover types, forested wetlands have the highest mean annual ET value (ca. 3.5 times that of urban covers) and contribute the highest amount to cumulative landscape ET. We critically note that this contribution (42%) by wetland forests is disproportionately higher (almost by a factor of 2) than their area coverage (23%). Herbaceous wetlands also have high mean annual ET and contribute 13.4% of the total cumulative ET. Agriculture has intermediate ET values relative to the other land uses and contributes 17.7% of the total cumulative ET, a percentage similar to its area proportion.

A forest-specific analysis demonstrates that all forest types other than forested wetlands have similar mean ET rates (920–961 mm; **Table 2**). Forested wetlands constitute 81% of the total forested area but contribute ca. 90% of the cumulative ET provided by all forest cover types. For urban subcategories, the range of mean annual ET rates was large (195 to 740 mm), with higher values in open space and low-intensity urban as expected due to lower impervious cover (**Table 3**).

#### 3.2. Changes in annual ET from land use change

We also generated two different mean annual rates (one for 2000 to 2009 and one for 2010 to 2018) to assess changes between these two time periods. **Fig. 4A** illustrates the pixel-specific differences between

these two periods (2010–2018 minus 2000–2009), where positive values indicate ET increases. The change is relatively small across the study area, which is concordant with the documented small change in land use during these two periods. However, there are some evident areas, albeit limited in spatial extent, with ET decreases (blue colors in **Fig. 4A**) likely reflecting conversion to urban cover. Indeed, ET changes for newly-urbanized pixels were significantly higher (and importantly negative) compared to the no-change pixel group (**Fig. 4B**). That is, urbanization generally resulted in lower ET values, explaining such locations in **Fig. 4A**, whereas the no-change pixels exhibited ET changes centered around zero. There were also some locations with ET increases between these two time periods, but to a lesser magnitude than the observed ET declines; such locations primarily represent wetland and agriculture areas, suggestive of changes in weather variables or water availability that warrants further investigation.

#### 3.3. Drivers and models of annual ET

Among tested regression models, quadratic polynomial regression performed best for each predictor variable. There was a negative, significant ( $R^2 = 0.5, p < 0.001$ ) relationship between annual ET and impervious cover when using the full data set. **Fig. 5A** illustrates this negative trend using a random subset of 200 pixels (50 for each major land use cover denoted with different colors), with a similar, albeit lower,  $R^2$  (0.34) to that of the entire dataset. As expected, urban areas have a high impervious cover and associated low ET rates. Interestingly, the other three groups have similar (and very low) impervious covers but clearly different ET values; however, the separation by land cover is clear, again with wetland forest exhibiting the highest annual ET rates. Differences among these three groups are likely due to other land cover attributes (canopy cover, depth to water table) that drive ET.

There was a positive, significant relationship ( $R^2 = 0.4, p < 0.001$ ) between mean annual ET and canopy cover percent, which is shown in **Fig. 5B** using a subset of 200 pixels and an  $R^2$  (0.35) similar to that of the entire dataset. Despite this general positive trend, land cover groups cluster together and clearly differ in ET even at similar canopy covers. Wetland forests have similar percent canopy cover compared to upland forests but much higher ET rates, likely due to shallow water tables and thus more water availability. Similarly, canopy cover percent is often similar between urban and agriculture pixels, but agriculture clearly has higher ET rates due to crop (not tree canopy) water use.

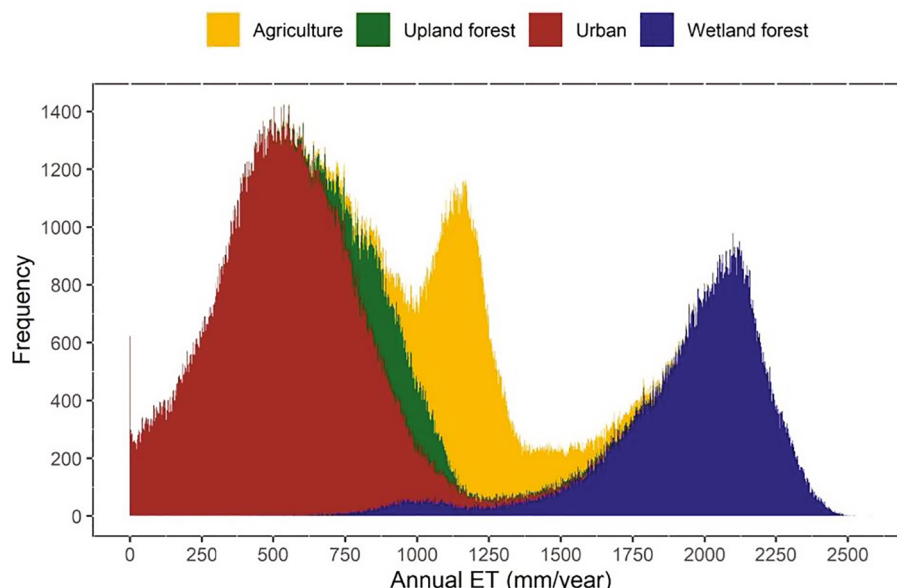


**Fig. 3.** Frequency distribution of annual ET values from all pixels categorized by major land use/cover.

**Table 1**

Percent of land area and mean, cumulative, and percent contributions of ET for major land use/cover types, where the percentages of land area and contributions are relative to the total landscape values. Grassland and barren land are excluded from the table due to their small area percentage (0.4% and 1%, respectively).

	Urban	Agriculture	Upland Forest	Forested Wetland	Herbaceous Wetland
Area (%)	45.42	16.42	5.48	23.46	9.22
<b>Evapotranspiration</b>					
Mean (mm)	546	1189	937	1945	1583
Cumulative ( $m^3$ )	$1.74 \times 10^8$	$1.36 \times 10^8$	$3.62 \times 10^7$	$3.20 \times 10^8$	$1.03 \times 10^8$
Contribution (%)	22.62	17.68	4.71	41.60	13.39

**Table 2**

Percent land area and mean, cumulative, and percent contributions for ET of each forest sub-types, where the percentages of land area and contributions are relative to the total forest cover.

	Deciduous Forest	Evergreen Forest	Mixed Forest	Shrub/Scrub	Forested Wetland
Area (%)	5.29	7.87	1.57	4.27	81.01
<b>Evapotranspiration</b>					
Mean (mm)	949	920	961	948	1945
Cumulative ( $m^3$ )	$1.02 \times 10^7$	$1.47 \times 10^7$	$3.07 \times 10^6$	$8.22 \times 10^6$	$3.20 \times 10^8$
Contribution (%)	2.86	4.13	0.86	2.31	89.84

**Table 3**

Percent land area and mean, cumulative, and percent contributions for ET of each urban sub-types, where the percentages of land area and contributions are relative to the total urban cover.

	Developed, Open Space	Developed, Low- Intensity	Developed, Medium- Intensity	Developed, High- Intensity
Area (%)	34.55	41.66	18.76	5.03
<b>Evapotranspiration</b>				
Mean (mm)	740	523	332	195
Cumulative ( $m^3$ )	$8.15 \times 10^7$	$6.95 \times 10^7$	$1.98 \times 10^7$	$3.12 \times 10^6$
Contribution (%)	46.86	39.96	11.38	1.80

There was a negative and significant ( $R^2 = 0.38, p < 0.001$ ) relationship between mean annual ET and depth to water table, suggesting that shallow water tables (small water table depth values) generally increase ET. The subset of 200 pixels illustrates this trend and with the same  $R^2$  value as the full dataset (0.38; Fig. 5C). Of the four major land covers, wetland forest generally has the smallest depths to water table (i.e., high water availability) and thus the highest ET values. However, there are some occurrences of upland forest and agriculture pixels with similar depth to water tables as wetland forest but with lower ET values; this is likely due to differences in canopy cover (see Fig. 5B). Likewise, urban pixels span similar ranges of water table depths as other categories but have substantially lower ET rates due to impervious cover. Together, these results highlight the interacting influences of multiple attributes (impervious cover, canopy cover, and water availability) on ET rates.

The best-fit multiple regression model for ET using impervious cover, canopy cover, and depth to water table was also a quadratic polynomial regression and is shown in Table 4. The resulting model had an  $R^2 = 0.71$ , with all variables significant and having similar relative importance. Fig. 6 illustrates this model with a subset of 100 pairs of predicted and observed values, with a similar  $R^2$  value to the entire dataset.

#### 4. Discussion

Using remotely sensed daily ET rates over a ca. 20-year time period, we compared annual ET among land cover types in Virginia Beach, a large urban landscape with growing stormwater flooding concerns. Such data enable ET estimation at both the spatial scales and resolution (30-m) necessary to inform stormwater planning and green infrastructure design. We found lower ET from urban covers and disproportional contributions from forest covers to total landscape ET, particularly from

wetland forests (i.e., ca. 40% of total land ET despite 20% of land area). Using higher resolution land use data, we were able to explain drivers of ET variation and develop predictive models for potential downscaling ET estimates. Our work indicates the potential value of urban forests in flood reduction and highlights how remotely sensed ET data can be used to inform stormwater planning and green infrastructure design.

#### 4.1. ET differences among and within land cover types

Relative differences in annual ET among land covers were evident, particularly when assessing each land cover's proportional contribution to total landscape ET (Table 1). As expected, urban rates had the lowest ET among all major land covers, consistent with other studies using remotely sensed estimates (Sun et al., 2004; Liu et al., 2010) and on-the-ground approaches (Liu et al., 2008). As a consequence, urban cover in Virginia Beach contributes only 23% of the total ET despite being the dominant land use (45% of area). To that end, we found significant ET decreases for newly urbanized pixels when parsing the ET dataset into two time periods (Fig. 4). Yet, there were also clear differences among urban sub-categories that highlight consequences of development intensity and continued changes thereof within urban areas. For example, ET values for open space and low intensity were 3.8 and 2.7 times higher compared to high intensity developed, respectively, and more comparable to (but less than) upland ET values (Tables 2 and 3). In Virginia Beach, and many other large mixed-land use landscapes, lower intensity urban areas can be dominant (approximately 35% of land area in Virginia Beach), suggesting their relative contribution to ET-associated functions and implications of continued development. These findings are supported by our regression analysis, where impervious cover decreased ET (Fig. 5A), and are in accordance with other studies exploring ET drivers in urban settings (Grimmond & Oke, 1999; Haase, 2009; Liu et al., 2010).

Upland and wetland forest covers exhibited much higher ET compared to urban areas, indicating the relative role of such forest patches in supporting ET-associated functions. In locations such as Virginia Beach and many others, growing stormwater flooding concerns are motivating both engineered and green infrastructure solutions (Soz, Kryspin-Watson, & Stanton-Geddes, 2016). The importance of "street" trees in runoff reduction has been recognized (Stovin, Jorgensen, & Clayden, 2008), but larger forest patches have received less attention as potential locations for flood mitigation services. Of particular note in our study area, wetland forests represent a major land cover (23% of the area) and are often adjacent to urban, flood-prone areas. We found that wetland forest covers have ET rates ca. 3.5 times that of urban, and thus

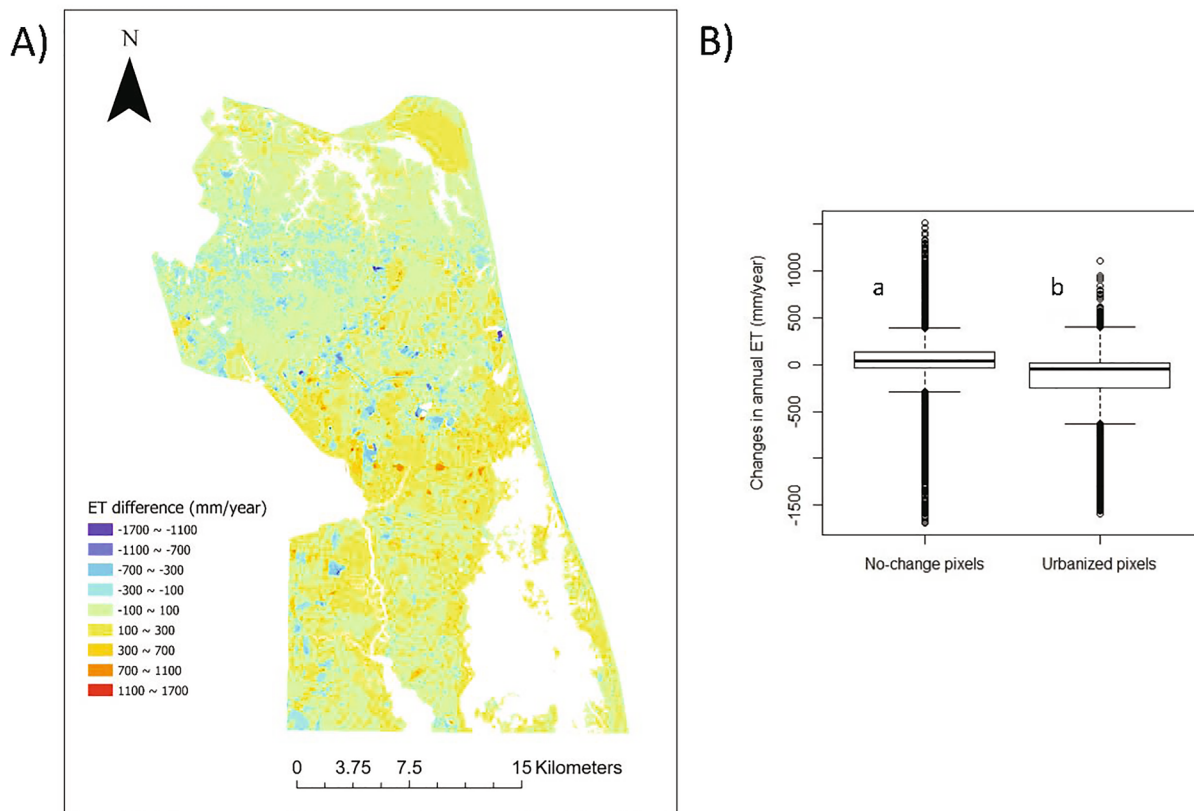


**Fig. 4.** A) Change in mean annual ET between 2000 and 2009 and 2010–2018, where positive values indicate ET increases (warm colors) and negative values indicate decreases (cool colors). B) Distribution of ET change values between 2000 and 2009 and 2010–2018 for pixels with no change in land use and pixels that were newly urbanized between these two time periods. Letters denote significant difference between pixel groups via Mann-Whitney-Wilcoxon Test.

disproportionately contribute to total landscape ET. Upland forests also exhibit higher rates than urban but lower than wetland forests, indicating important differences among forest cover types similar to those within the broad urban cover class. Regression analysis highlighted the influence of water table depth on ET (Fig. 5c), helping to explain higher ET in wetland forests where water availability increases ET rates. Canopy cover can also exert a strong control on forest ET rates (Fig. 5B), and accordingly many ET predictive models are largely based on such forest structural attributes, including basal area and leaf area index (Yan et al., 2012; McLaughlin, Kaplan, & Cohen, 2013). However, such modeling and targeted urban forest conservation may benefit from a better representation of the ET differences among forest types due to forest composition, canopy structure, and water availability.

#### 4.2. Tools to guide urban forest conservation

Our findings regarding ET differences between forested and urban areas are not surprising, but we emphasize the magnitude of those differences and, importantly, how such information can support tools to assess and incorporate the role of urban forests in stormwater planning. For example, remotely sensed ET data can enable estimates of ET change with forest loss scenarios and thus demonstrate the value of forest conservation as an important green infrastructure strategy. As of 2020, approximately half of Virginia Beach forests were either protected (reported by the Virginia Department of Conservation and Recreation) or controlled by the City of Virginia Beach. For the remaining “unprotected” forests, replacing pixel-specific ET observations with mean values for different urban subcategories yields annual ET losses of 11% – 32% compared to current total forest ET, the range of which depends on development intensity (data not shown). Going forward, ET data can support such scenario analyses for particular locations relevant for

specific land planning decisions. Further, integrating ET observations with higher resolution land attribute data can guide planning decisions at smaller spatial scales and potentially inform stormwater models and policies. Aggregating data for impervious and canopy covers (0.5 m resolution) and water table depth (3-m), we developed a multiple regression model that explained 71% of the variation in 30-m annual ET estimates. Such predictive models thus have the potential to use increasingly available fine-scale land use data for ET downscaling and to inform such actions as stormwater credit programs, which often occur at sub-30 m scales.

We focused on ET services in the context of flood reduction given the pressing stormwater concerns in Virginia Beach and other urban landscapes, yet urban forest ET supports additional functions. For example, urban forest patches have been shown to mitigate urban overheating, largely due to elevated ET and thus latent heat exchange (Hiemstra, Saaroni, & Amorim, 2017). As such, urban forests can serve as “cool spots”, the extent to which can be indicated by relative ET estimates compared to other land covers. Further, ET, particularly in vegetated covers where transpiration dominates the flux, is directly linked to carbon uptake rates (Scott, Huxman, Cable, & Emmerich, 2006) thereby indicating potential carbon sequestration rates. Thus, our work and others focusing on urban forest ET has direct relevance to valuing multiple ecosystem services. Last, and not necessarily linked to ET, urban forests provide additional functions (e.g., habitat provision, recreation, water and air quality; Mörberg, 2001; Arnberger, 2006; Livesley, McPherson, & Calfapietra, 2016; Nowak, 2016), and quantified ET rates can help add to the portfolio of urban forest services and thus guide urban forest conservation and management.

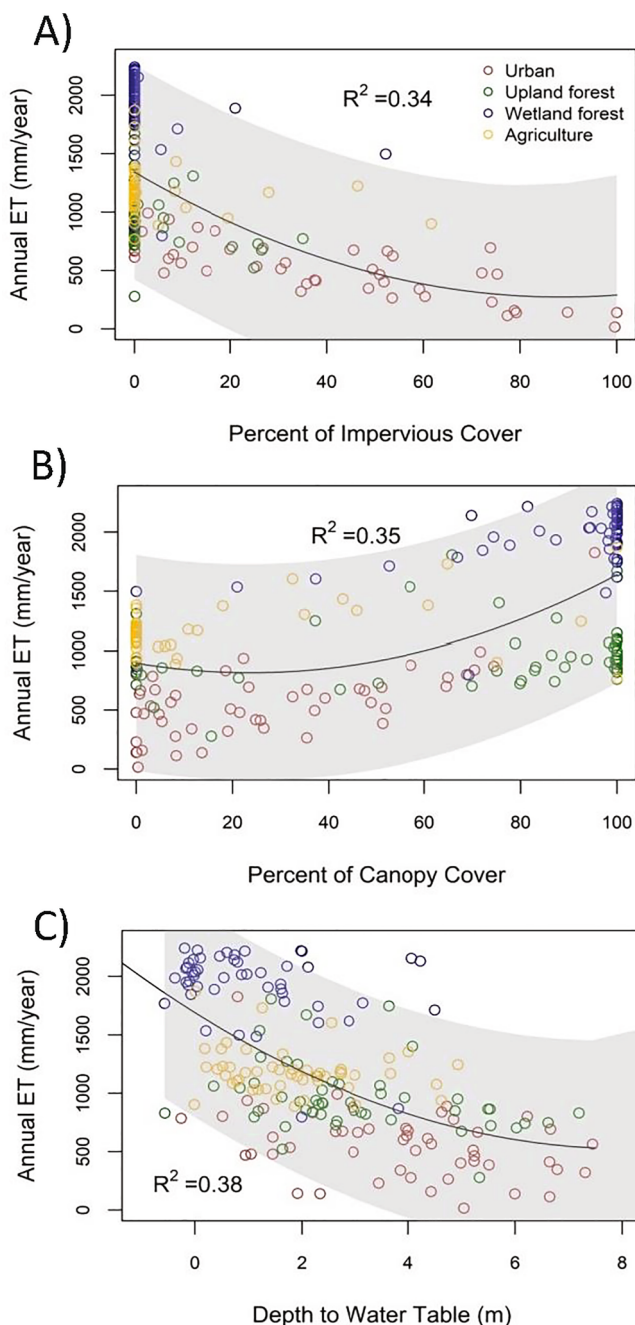


**Fig. 5.** Mean annual ET versus A) percent impervious cover, B) percent canopy cover, and C) depth to water table for a subset of 200 randomly sampled pixels and equally from four major land uses (denoted by colors). Note that a negative depth to water table value represents standing water. Grey area represents 95% confidence interval.

#### 4.3. Limitations and future work

There are several limitations of our study that warrant future work. First, while there are multiple remotely sensed ET methods (Nouri, Beecham, Anderson, Hassanli, & Kazemi, 2015), we used METRIC-derived ET data given its longer record and higher spatial resolution compared to that of other currently available datasets, such as the MOD16 global ET product (500-m) and the Global Land Data Assimilations ET product (ca. 28 km). However, the METRIC model has had limited applications in urban settings, and some studies have suggested improvements to it and other energy-based approaches to quantify ET

**Table 4**

Summary of the quadratic polynomial regression model predicting mean annual ET with three predictor variables: impervious cover, canopy cover, and depth to water table. The Relative Importance metric represents the relative  $R^2$  contribution among regressors following Lindemmen et al. (1980).

Summary of Fit						
Multiple R	0.71					
Square						
Adjusted R	0.71					
Square						
Residual	337.9					
Standard						
Error						
Observations	713,754					
Parameter Estimates						
Term	Estimate	Std Error	t-value	Prob >  t		Relative Importance
Intercept	1368	0.81	1685.26	<0.0001		
Impervious cover percent	-13.44	0.056	-238.94	<0.0001	0.17	
Impervious cover percent <sup>2</sup>	0.068	0.00068	99.95	<0.0001	0.10	
Water table depth	-119.5	0.27	-450.98	<0.0001	0.17	
Water table depth <sup>2</sup>	2.79	0.016	172.07	<0.0001	0.023	
Canopy cover percent	-5.24	0.049	-107.28	<0.0001	0.10	
Canopy cover percent <sup>2</sup>	0.11	0.0005	223.07	<0.0001	0.14	

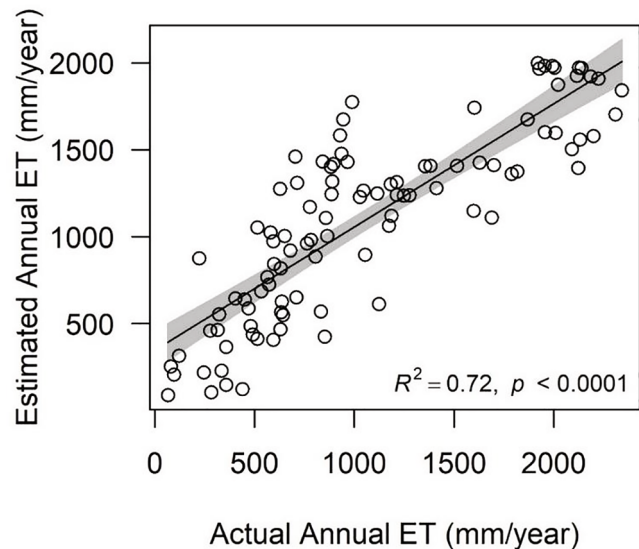


**Fig. 6.** Modeled versus actual annual ET for a subset of 100 randomly selected pixels, where the modeled values use impervious cover, canopy cover, and depth to water table.

for impervious covers (Zhang et al., 2017; Faridatul et al., 2020). For example, Faridatul et al. (2020) refined the SEBAL method to represent urban land surface parameters and anthropogenic heat fluxes, terming the new model uSEBAL. Applying both models in a mixed-land use landscape, the authors found similar values between SEBAL and uSEBAL for vegetated covers but lower ET estimates from the new model for impervious covers. Given that METRIC is largely based off of SEBAL, similar refinements to METRIC may also result in little change in urban forest ET estimates but lower rates for urban covers, further increasing the differences among these land covers as observed in our study. We also note that in situ ET estimates were not available in our study for model validation, representing an additional limitation of our work and

future needs to validate METRIC in urban and suburban systems. Further, the METRIC model relies on the selection of hot (i.e., low ET) pixels and cold (i.e., high ET) pixels for boundary conditions of ET extremes. Accordingly, hot pixels are selected as those with the highest surface temperatures and least vegetated areas (via NDVI), whereas cool pixels represent areas with the lowest temperature and highest NDVI values, such that pixel selection is image dependent (Allen et al., 2013). While there is consensus for cold pixel selection, hot pixel selection approaches have been debated. For example, Lian and Huang (2015) suggest that sub-image hot pixel selection may be more appropriate for images with different surface thermal characteristics. Mixed land uses widely vary in surface properties, and the sensitivity of ET estimates to pixel selection in such settings remains uncertain, highlighting future work needs.

With these limitations of the METRIC model acknowledged, we suggest that the observed magnitude of relative ET differences among land covers helps to reduce the uncertainty from its application in our mixed-land use study site. Further, we again note the observed relationships between annual ET and expected drivers derived from an independent dataset, adding credence to our general findings. Nonetheless, we, like other researchers (Nouri et al., 2015; Zhang et al., 2017; Faridatul et al., 2020), emphasize the need to further validate and refine remotely sensed ET methods for heterogeneous landscapes and, in doing so, increase the data availability from such methods.

There are also considerations for deriving annual rates from (16-day frequency) daily ET records. Specifically, we screened both cloudy scenes and cloud-contaminated pixels to remove associated errors in ET estimates. While this is typically conducted (Tsouni, Kontoes, Koutsoyiannis, Elias, & Mamassis, 2008; Senay et al., 2016), it results in a systematic bias for high ET days since cloud cover decreases solar radiation and increases relative humidity, both of which result in lower daily ET rates (Zhang, Wang, Wang, & Zhang, 2016). Indeed, some of our annual rates for wetland forests approached 2,500 mm/yr, representing extreme values (compared to PET = 800 – 900 mm/yr in the region). Observed ET rates can often exceed PET due to such phenomena as the clothesline and oasis effects (Drexler et al., 2004). Nonetheless, our annual rates likely remain overestimates by biasing our dataset to cloud-free days. Such bias can be reduced by constructing pixel-specific relationships between (cloud-free) daily ET observations and climate-based PET estimates, where developed relationships and daily PET are then subsequently used to estimate daily ET time series (e.g., Singh, Liu, Tieszen, Suyker, & Verma, 2012). However, given our objective, we decided against this approach, suggesting it may introduce additional uncertainty (Lepot, Aubin, & Clemens, 2017). That is, our objective was to compare ET rates among land covers in one landscape, and we contend that relative differences in ET (via annual estimates solely using cloud-free days) are maintained and informative in understanding ET drivers and differences among land covers. Where absolute annual ET estimates are the objective (e.g., for water budget calculations, hydrologic model inputs, and comparisons to other regions), developing ET-PET relationships for estimating complete daily ET time series is the more appropriate approach.

Last, our work estimated relative differences in annual ET among land uses but did not quantify the runoff reductions that may be realized. While runoff reduction is expected with higher ET (Rossi, Whipple, & Vivoni, 2016), specifically within urban forests, the degree to which annual ET estimates affect runoff reduction remains largely unknown, particularly at storm-event scales. In low-relief landscapes such as Virginia Beach, saturation-excess runoff (i.e., shallow water tables limiting infiltration) can be the dominant form of runoff (Appels, Bogaart, & van der Zee, 2016). Thus, runoff potential for any given storm event is determined by antecedent water table and soil moisture levels (Hernandez, Nachabe, Ross, & Obeysekera, 2003), which are largely regulated by preceding ET water losses (Gerla, 1992). This supports the notion that higher ET will lead to runoff reduction and underscores a need to better parameterize commonly used stormwater models (e.g.,

Storm Water Management Model; SWMM) to represent ET differences and drivers among land cover types. Indeed, most applications of SWIMM simulate time-varying ET using climate data and apply the same rate across the model domain, failing to represent land cover ET controls (but see Feng & Burian, 2016). To do so will require daily ET time series and therefore ET-PET modeling as discussed above. Thus, our estimates of annual ET differences only point to this research need and the potential for forest runoff reduction services, but do not provide the requisite data for such stormwater modeling efforts.

## 5. Conclusions

In this work, we used remotely sensed, 30-m ET data for a large, mixed-land use urban landscape (Virginia Beach, USA) and demonstrated large differences in annual ET values between land cover types. Variation in ET among land covers is well recognized, but our work highlights the potential utility of remotely sensed ET data to better incorporate urban forests in stormwater planning and green infrastructure design. For example, wetland forests, the dominant forest cover in Virginia Beach, have the highest ET rates among all land cover types (roughly 3.5 times that of urban) and contribute ca. 40% of the cumulative landscape ET but only ca. 20% of the land area. Such observed ET differences among land covers can be used in land use change scenarios to prioritize specific locations for urban forest conservation. We also found significant relationships between annual ET and higher resolution land attribute data, providing a potential approach to downscale ET estimates and thus further inform stormwater planning at smaller spatial scales, including such policies as stormwater crediting. However, future work is needed to better represent land cover ET differences within stormwater models for quantifying potential runoff reduction. Our work may help to motivate such future work but hopefully, at hand, will guide urban forest conservation efforts as part of the increasing use of green infrastructure solutions for multiple ecosystem services.

## Acknowledgements

This work was funded by The Nature Conservancy and the City of Virginia Beach.

## References

- Adnan, S., Ullah, K., Khan, A. H., & Gao, S. (2017). Meteorological impacts on evapotranspiration in different climatic zones of Pakistan. *J. Arid Land*, *9*, 938–952. <https://doi.org/10.1007/s40333-017-0107-2>.
- Allen, R. G., Tasumi, M., Morse, A., Trezza, R., Wright, J. L., Bastiaanssen, W., ... Robison, C. W. (2007). Satellite-based energy balance for mapping evapotranspiration with internalized calibration (METRIC)—Applications. *Journal of Irrigation and Drainage Engineering*, *133*, 395–406.
- Allen, R., Irmak, A., Trezza, R., Hendrickx, J. M., Bastiaanssen, W., & Kjaersgaard, J. (2011). Satellite-based ET estimation in agriculture using SEBAL and METRIC. *Hydrological Processes*, *25*, 4011–4027.
- Allen, R. G., Burnett, B., Kramer, W., Huntington, J., Kjaersgaard, J., Kilic, A., ... Trezza, R. (2013). Automated calibration of the metric-landsat evapotranspiration process. *JAWRA Journal of the American Water Resources Association*, *49*, 563–576.
- Allen, R. G., Morton, C., Kamble, B., Kilic, A., Huntington, J., Thau, D., et al. (2015). EEflux: A Landsat-based evapotranspiration mapping tool on the Google Earth Engine. I: 2015 ASABE/IA Irrigation Symposium: Emerging Technologies for Sustainable Irrigation-A Tribute to the Career of Terry Howell, Sr. Conference Proceedings. American Society of Agricultural and Biological Engineers, pp. 1–11.
- Appels, W. M., Bogaart, P. W., & van der Zee, S. E. (2016). Surface runoff in flat terrain: How field topography and runoff generating processes control hydrological connectivity. *Journal of Hydrology*, *534*, 493–504.
- Arnberger, A. (2006). Recreation use of urban forests: An inter-area comparison. *Urban Forestry & Urban Greening*, *4*, 135–144.
- Berland, A., Shiflett, S. A., Shuster, W. D., Garmestani, A. S., Goddard, H. C., Herrmann, D. L., & Hopton, M. E. (2017). The role of trees in urban stormwater management. *Landscape and Urban Planning*, *162*, 167–177.
- Chen, H., & Yang, D. (2012). Remote sensing based continuous estimation of regional evapotranspiration by improved SEBS model. In *Land Surface Remote Sensing (p. 85240M)*. International Society for Optics and Photonics.
- Courault, D., Seguin, B., & Olioso, A. (2005). Review on estimation of evapotranspiration from remote sensing data: From empirical to numerical modeling approaches. *Irrigation and Drainage Systems*, *19*, 223–249.

- De Roo, A., Schmuck, G., Perdigao, V., & Thielen, J. (2003). The influence of historic land use changes and future planned land use scenarios on floods in the Oder catchment. *Physics and Chemistry of the Earth, Parts A/B/C*, 28, 1291–1300.
- DiGiovanni-White, K., Montalto, F., & Gaffin, S. (2018). A comparative analysis of micrometeorological determinants of evapotranspiration rates within a heterogeneous urban environment. *Journal of Hydrology*, 562, 223–243.
- Dormann, C. F., McPherson, J. M., Araujo, M. B., Bivand, R., Bolliger, J., ... Wilson, R. (2007). Methods to account for spatial autocorrelation in the analysis of species distributional data: a review. *Ecography*, 30, 609–628.
- Drexler, J. Z., Snyder, R. L., Spano, D., & Paw U, K. T. (2004). A review of models and micrometeorological methods used to estimate wetland evapotranspiration. *Hydrological Processes*, 18, 2071–2101.
- Faridatul, M., Wu, B., Zhu, X., & Wang, S. (2020). Improving remote sensing based evapotranspiration modelling in a heterogeneous urban environment. *Journal of Hydrology*, 581, Article 124405.
- Foolad, F., Blankenau, P., Kilic, A., Allen, R.G., Huntington, ... Ratcliffe, I. (2018). Comparison of the automatically calibrated google evapotranspiration application—EEFlux and the manually calibrated METRIC application.
- Feng, Y., & Burian, S. (2016). Improving evapotranspiration mechanisms in the U.S. Environmental Protection Agency's Storm Water Management Model. *Journal of Hydrologic Engineering*, 12, 06016007.
- French, A. N., Hunsaker, D. J., & Thorp, K. R. (2015). Remote sensing of evapotranspiration over cotton using the TSEB and METRIC energy balance models. *Remote Sensing of Environment*, 158, 281–294.
- Gerla, P. J. (1992). The relationship of water-table changes to the capillary fringe, evapotranspiration, and precipitation in intermittent wetlands. *Wetlands*, 12, 91–98.
- Glenn, E. P., Doody, T. M., Guerschman, J. P., Huete, A. R., King, E. A., McVicar, T. R., ... Zhang, Y. (2011). Actual evapotranspiration estimation by ground and remote sensing methods: The Australian experience. *Hydrological Processes*, 25, 4103–4116.
- Gowda, P. H., Chavez, J. L., Colaizzi, P. D., Evett, S. R., Howell, T. A., & Tolk, J. A. (2007). Remote sensing based energy balance algorithms for mapping ET: Current status and future challenges. *Transactions of the ASABE*, 50, 1639–1644.
- Grimmond, C. S., & Oke, T. R. (1991). An evapotranspiration model for urban areas. *Water Resources Research*, 27, 1739–1755.
- Grimmond, C. S., & Oke, T. R. (1999). Evapotranspiration rates in urban areas. *IAHS Publication*, 259, 235–244.
- Haase, D. (2009). Effects of urbanisation on the water balance—A long-term trajectory. *Environmental Impact Assessment Review*, 29, 211–219.
- Hernandez, T., Nachabe, M., Ross, M., & Obeysekera, J. (2003). Modeling runoff from variable source areas in humid, shallow water table environments. *Journal of the American Water Resources Association*, 39, 75–85.
- Hiemstra, J. A., Saaroni, H., & Amorim, J. H. (2017). The urban heat Island: Thermal comfort and the role of urban greening. *The Urban Forest*. Springer, 7–19.
- Hwang, K., & Choi, M. (2013). Seasonal trends of satellite-based evapotranspiration algorithms over a complex ecosystem in East Asia. *Remote Sensing of Environment*, 137, 244–263.
- Irmak, S., Haman, D.Z. (2003). Evapotranspiration: potential or reference. IFAS Extension, ABE 343.
- Kişi, Ö. (2006). Generalized regression neural networks for evapotranspiration modelling. *Hydrological Sciences Journal*, 51, 1092–1105.
- Kişi, Ö. (2011). Evapotranspiration modeling using a wavelet regression model. *Irrigation Science*, 29, 241–252.
- Kuehler, E., Hathaway, J., Tirpak, A. (2017). Quantifying the benefits of urban forest systems as a component of the green infrastructure stormwater treatment network. *Ecohydrology*, 10, 10.1002/eco.1813.
- Larguech, F. B. (2006). Estimating soil contamination with kriging interpolation method. *American Journal of Applied Sciences*, 3, 1894–1898.
- Lennon, M., Scott, M., & O'Neill, E. (2014). Urban design and adapting to flood risk: The role of green infrastructure. *Journal of Urban Design*, 19, 745–758.
- Lepot, M., Aubin, J.-B., & Clemens, F. H. (2017). Interpolation in time series: An introductory overview of existing methods, their performance criteria and uncertainty assessment. *Water*, 9, 796.
- Lian, J., & Huang, M. (2015). Evapotranspiration estimation for an oasis area in the Heihe River Basin using Landsat-8 images and the METRIC Model. *Water Resources Management*, 29, 5157–5170.
- Litvak, E., Manago, K., Hogue, T., & Pataki, D. (2017). Evapotranspiration of urban landscapes in Los Angeles, California at the municipal scale. *Water Resources Research*, 53, 4236–4252.
- Liu, M., Tian, H., Chen, G., Ren, W., Zhang, C., & Liu, J. (2008). Effects of land-use and land-cover change on evapotranspiration and water yield in China during 1900–2000 I. *Journal of the American Water Resources Association*, 44, 1193–1207.
- Lu, W., Hong, Y., Khan, S. I., Huang, M., Vieux, B., Caliskan, S., & Grout, T. (2010). Actual evapotranspiration estimation for different land use and land cover in urban regions using Landsat 5 data. *Journal of Applied Remote Sensing*, 4, Article 041873.
- Lu, W., Chen, W., & Peng, C. (2014). Assessing the effectiveness of green infrastructures on urban flooding reduction: A community scale study. *Ecological Modelling*, 291, 6–14.
- Livesley, S. J., McPherson, E. G., & Calfapietra, C. (2016). The urban forest and ecosystem services: Impacts on urban water, heat, and pollution cycles at the tree, street, and city scale. *Journal of Environmental Quality*, 45, 119–124.
- Lu, J., Sun, G., McNulty, S. G., & Amatya, D. M. (2003). Modeling actual evapotranspiration from forested watersheds across the Southeastern United States. *Journal of the American Water Resources Association*, 39, 886–896.
- McLaughlin, Daniel, Kaplan, David, & Cohen, Matthew (2013). Managing forests for increased regional water yield in the southeastern U.S. coastal plain. *Journal of the American Water Resources Association*, 49(4), 953–965. <https://doi.org/10.1111/jawr.12073>.
- Mörting, U. M. (2001). Resident bird species in urban forest remnants; landscape and habitat perspectives. *Landscape Ecology*, 16, 193–203.
- Nowak, D. (2016). Urban forests. In Robertson, G., Mason, A., eds. Assessing the sustainability of agricultural and urban forests in the United States. USDA Forest Service FS-1067, Washington, DC: 37-52, 37–52.
- Nowack, D. J., Noble, M. H., Sisinni, S. M., & Dwyer, J. F. (2001). People and trees: assessing the US urban forest resource. *Journal of Forestry*, 99, 37–42.
- Nouri, H., Beecham, S., Anderson, S., Hassanli, A., & Kazemi, F. (2015). Remote sensing techniques for predicting evapotranspiration from mixed vegetation surfaces. *Urban Water Journal*, 12, 380–393.
- Nouri, H., Glenn, E., Beecham, S., Boroujeni, S., Sutton, P., Alaghmand, S., ... Nagler, P. (2016). Comparing three approaches of evapotranspiration estimation in mixed urban vegetation: Field-based, remote sensing-based and observational-based methods. *Remote Sensing*, 9, <https://doi.org/10.3390/rs8060492>.
- Nouri, H., Nagler, P., Boroujeni, S., Munoz, A., Sutton, P., Alaghmand, S., ... Didan, K. (2020). Effect of spatial resolution of satellite images on estimating the greenness and evapotranspiration of urban green spaces. *Hydrological Processes*, 34, 3183–3199.
- Soil Survey Staff, Natural Resources Conservation Service, Unites States Department of Agriculture. Soil Survey Geographic (SSURGO) Database. <https://sdmdataaccess.sc.egov.usda.gov>. (accessed 10 September, 2019).
- O'Neil-Dunne. (2019). Tree Canopy Change Assessment, Virginia Beach, 2012–2018. Study by the University of Vermont.
- Peters, E., Hiller, R., & McFadden, J. (2011). Seasonal contributions of vegetation types to suburban evapotranspiration. *Journal of Geophysical Research*, 116, G010003.
- Qiu, S., Zhu, Z., & He, B. (2019). Fmask 4.0: Improved cloud and cloud shadow detection in Landsats 4–8 and Sentinel-2 imagery. *Remote Sensing of Environment*, 231, Article 111205.
- Rossi, M. W., Whipple, K. X., & Vivoni, E. R. (2016). Precipitation and evapotranspiration controls on daily runoff variability in the contiguous United States and Puerto Rico. *Journal of Geophysical Research: Earth Surface*, 121, 128–145.
- Rothfuss, Y., Biron, P., Braud, I., Canale, L., Durand, J.-L., Gaudet, J.-P., ... Bariac, T. (2010). Partitioning evapotranspiration fluxes into soil evaporation and plant transpiration using water stable isotopes under controlled conditions. *Hydrological Processes*, 24, 3177–3194. <https://doi.org/10.1002/hyp.7743>.
- Sanford, W. E., & Selnick, D. L. (2013). Estimation of evapotranspiration across the conterminous United States using a regression with climate and land-cover data 1. *JAWRA Journal of the American Water Resources Association*, 49, 217–230.
- Scott, R. L., Huxman, T. E., Cable, W. L., & Emmerich, W. E. (2006). Partitioning of evapotranspiration and its relation to carbon dioxide exchange in a Chihuahuan Desert shrubland. *Hydrological Processes: An International Journal*, 20, 3227–3243.
- Senay, G. B., Friedrichs, M., Singh, R. K., & Velpuri, N. M. (2016). Evaluating Landsat 8 evapotranspiration for water use mapping in the Colorado River Basin. *Remote Sensing of Environment*, 185, 171–185.
- Shao, Y., Li, G. L., Guenther, E., & Campbell, J. B. (2015). Evaluation of topographic correction on subpixel impervious cover mapping with CBERS-2B data. *IEEE Geoscience and Remote Sensing Letters*, 12, 1675–1679.
- Singh, R. K., Liu, S., Tieszen, L. L., Suyker, A. E., & Verma, S. B. (2012). Estimating seasonal evapotranspiration from temporal satellite images. *Irrigation Science*, 30, 303–313.
- Spiliopoulos, M., Holden, N., & Loukas, A. (2017). Mapping evapotranspiration coefficients in a temperate maritime climate using the METRIC Model and Landsat TM. *Water*, 9, Article w9010023.
- Soz, S. A., Kryspin-Watson, J., & Stanton-Geddes, Z. (2016). *The role of green infrastructure solutions in urban flood risk management*. Washington, DC: World Bank.
- Stovin, V. R., Jorgensen, A., & Clayton, A. (2008). Street trees and stormwater management. *Arboricultural Journal*, 30, 297–310.
- Sun, R., Chen, J. M., Zhu, Q., Zhou, Y., Liu, J., Li, J., ... Tang, S. (2004). Spatial distribution of net primary productivity and evapotranspiration in Changbaishan Natural Reserve, China, using Landsat ETM+ data. *Canadian Journal of Remote Sensing*, 30, 731–742.
- Taha, H. (1997). Urban climates and heat islands: Albedo, evapotranspiration, and anthropogenic heat. *Energy and Buildings*, 25, 99–103.
- Teuling, A. J., Hirschi, M., Ohmura, A., Wild, M., Reichstein, M., Ciais, P., ... Richardson, A. D. (2009). A regional perspective on trends in continental evaporation. *Geophysical Research Letters*, 36, L02404.
- Trezzia, R., Allen, R. G., & Tasumi, M. (2013). Estimation of actual evapotranspiration along the Middle Rio Grande of New Mexico using MODIS and landsat imagery with the METRIC model. *Remote Sensing*, 5, 5397–5423.
- Tsouni, A., Kontoes, C., Koutsogiannis, D., Elias, P., & Mamassis, N. (2008). Estimation of actual evapotranspiration by remote sensing: Application in Thessaly Plain, Greece. *Sensors*, 8, 3586–3600.
- [dataset] U.S. Census Bureau QuickFacts: Virginia Beach city, Virginia (County), n.d. <https://www.census.gov/quickfacts/virginiateachcityvirginiacounty> (accessed 23, May, 2019).
- Wu, C., & Murray, A. T. (2003). Estimating impervious surface distribution by spectral mixture analysis. *Remote Sensing of Environment*, 84, 493–505.
- Yan, H., Wang, S. Q., Billesbach, D., Oechel, W., Zhang, J. H., Meyers, T., ... Bohrer, G. (2012). Global estimation of evapotranspiration using a leaf area index-based surface energy and water balance model. *Remote Sensing of Environment*, 124, 581–595.

- Zhang, L., Dawes, W. R., & Walker, G. R. (2001). Response of mean annual evapotranspiration to vegetation changes at catchment scale. *Water Resources Research*, 37, 701–708. <https://doi.org/10.1029/2000WR000000>.
- Zhang, Q., Wang, W., Wang, S., & Zhang, L. (2016). Increasing trend of pan evaporation over the semiarid loess plateau under a warming climate. *Journal of Applied Meteorology and Climatology*, 55, 2007–2020.
- Zhang, Y., Li, L., Chen, L., Liao, Z., Wang, Y., Wang, B., & Yang, X. (2017). A modified multi-source parallel model for estimating urban surface evapotranspiration based on ASTER thermal infrared data. *Remote Sensing*, 9, 1029.